New Poly(phenylene oxide)/Polystyrene Blend Nanocomposites with Clay: Intercalation, Thermal and Mechanical Properties

Rajkiran R. Tiwari,[1] Kartic C. Khilar,[2] Upendra Natarajan[1]

[1]*Polymer Science and Engineering Division, National Chemical Laboratory, Pune 411008, India*
[2]*Department of Chemical Engineering, Indian Institute of Technology, Bombay, Powai, Mumbai 400076, India*

Received 8 June 2007; accepted 6 November 2007
DOI 10.1002/app.27743
Published online 29 January 2008 in Wiley InterScience (www.interscience.wiley.com).

ABSTRACT: We present the first study and results on the preparation and characterization of montmorillonite clay filler based polymer blend nanocomposites of the miscible poly(phenylene oxide)/polystyrene blend. Intercalated nanocomposites, prepared by a melt-processing method with 2–6 wt % commercially available organically modified sodium montmorillonite, have been characterized with wide-angle X-ray diffraction, transmission electron microscopy analysis, thermal analysis (thermogravimetric analysis and differential scanning calorimetry), and mechanical tensile tests. We show that nanocomposites can be successfully prepared in a batch mixer at temperatures much below the conditions conventionally used for this blend without organic degradation. Thermal stability is enhanced by nanoscale hybrid formation. The level of intercalation (change in the *d*-spacing) does not change with the clay loading. Better dispersion of clay in the blend matrix has been observed at a low level of clay content. The nanocomposites show improved tensile modulus (by 31%) in comparison to the blend, whereas the tensile strength (stress at break) and elongation decrease in the presence of the filler with an increase in the clay loading. The Halpin–Tsai model is able to predict the modulus of the nanocomposites in very good agreement with the experimental data. © 2008 Wiley Periodicals, Inc. J Appl Polym Sci 108: 1818–1828, 2008

Key words: mechanical properties; nanocomposites; organoclay; poly(phenylene oxide); polystyrene; thermal properties

INTRODUCTION

Research in the field of polymer-layered silicate nanocomposites has gained tremendous importance in recent years as a result of enhancements in thermal stability and mechanical properties for such advanced materials.[1–4] The pioneering work of researchers at Toyota led to the discovery of nanoscale polymer–clay nanocomposites as candidates for light-weight-material applications.[5,6] Most commonly known thermoplastic polymers have been investigated either in an exploratory manner or in depth for their structure and morphology, thermal behavior, mechanical properties, dynamic behavior, and so forth.

At this time, very few publications in the literature have reported nanocomposites of polymer blends and clay. Li and Shimizu[7] looked at poly(phenylene oxide) (PPO)/polyamide 6 (PA6) blend nanocomposites by melt mixing. They obtained a significant decrease in the domain size of the dispersed PPO phase in the presence of organoclays. However, an increase in the organoclay loading (>5 wt %) led to the formation of a cocontinuous morphology.[7] Gelfer et al.[8] prepared nanocomposites of the immiscible polystyrene (PS)/poly(methyl methacrylate (PMMA) blend by a melt-mixing process, using commercially available dimethyl dioctadecyl ammonium modified montmorillonite. The presence of the organoclay partially compatibilizes the immiscible PS/PMMA blend by reducing the average microdomain size (from 1–1.5 μm to ca. 300–500 nm).[8] The area of polymer blend–clay nanocomposites is open to considerable research with the possibility of providing very interesting fundamental and practical progress. The structure–property relationships in the case of advanced materials formed by polymer blends and clays can be even more challenging with respect to property variations, control, and tailoring with molecular parameters and design.

Tensile strength, thermal stability, and flame retardancy are desirable properties for machine and appliance housings. PPO and PS are amorphous and

Correspondence to: U. Natarajan (u.natarajan@ncl.res.in or upen.natarajan@gmail.com).

Contract grant sponsor: Council of Scientific and Industrial Research of India (through a graduate senior research fellowship to R.R.T.).

molecularly miscible over all compositions of either PPO or PS, as observed with various characterization techniques such as optical and mechanical studies and electron microscopy.[9–11] PPO, along with PS, exhibits a broad range of outstanding properties for applications in computers and business equipment, the automotive industry, electrical insulation, telecommunications, electronics, and many other industries. PS is brittle, whereas PPO is a ductile polymer, and the transition from a brittle material to a ductile material occurs with >25 wt % PPO in the PPO/PS blend.[12] Chun and Gibala[12] studied the mechanical properties of the PPO/PS blend with various compositions and observed a linear increase in the break stress with an increase in PPO in the blend accompanied by a slightly positive deviation at a higher PPO fraction. A synergistic effect was observed in the PPO/PS blend with the maximum tensile modulus observed at 50 wt % PPO, with the increase in the modulus attributed to the increase in the specific intermolecular interactions between PPO and PS, which led to high modulus and yield stress and a reduction in the strain at break.[12] However, for the strain at break, a negative deviation from linear behavior was observed. The positive deviation for tensile properties was mainly due to specific interactions between PPO and PS causing a loss in the free volume of the blend, which further led to higher modulus and tensile strength.[13,14] In comparison, Costa and Oliveira[15] prepared a partially miscible/compatible blend of PA6 and PPO by solution blending and observed the maximum tensile modulus and tensile strength at a PA6 content of 99%. The improvement with as little as 1 wt % PPO was due to its antiplasticizing effect. At a higher percentages of PPO, the elongation at break improved, whereas the tensile modulus and tensile strength were reduced.[15] Tjong and Ke[13] studied the blend of PPO and high-impact polystyrene (HIPS) by injection molding and observed positive deviation behavior for the yield strength and modulus at all compositions of HIPS.

The prime motivation of this study is to investigate the structural, thermal, and mechanical properties of molecularly miscible PPO/PS blend–organoclay nanocomposites. We show that intercalated nanocomposites are formed with quaternary ammonium cations having a dominant aliphatic nature. The effects of organoclays and their fraction in the matrix on the nanoscale structure and thermal and mechanical properties of the hybrids are discussed. The PPO/PS system is attractive and relatively simple to use as a model blend system for polymer–clay nanocomposite studies as morphological complications arising from immiscibility are absent in this case. To our knowledge, this report is the first study of the PPO/PS system and shows that nanocomposites can be formed with improved properties by the suitable choice of processing conditions.

EXPERIMENTAL

Materials and nanocomposite preparation

Cloisite 10A was supplied by Southern Clay Products, Inc. (Texas), as a complimentary gift. Cloisite 10A is an organically modified montmorillonite containing dimethylbenzyl hydrogenated tallow quaternary ammonium ion as an organic modifier. Cloisite 10A is an overexchanged organomontmorillonite with a relatively high cation-exchange capacity of 125 mequiv/100 g. The hydrogenated tallow contains an alkyl chain length varying from C14 to C18. The typical composition of the different chain lengths is $\sim$ 65% C18 (dominant), $\sim$ 30% C16, and $\sim$ 5% C14.

The PPO/PS blend (grade Noryl 701) was a commercial sample supplied by General Electric, Inc. (USA), and was obtained in the form of pellets and used as is without any further modifications. On the basis of the measurement of the glass-transition temperature (T_g) of this blend, the composition of the PPO/PS blend, as calculated with the Fox equation, was 80.51 wt % PS and 19.49 wt % PPO. The T_g values of PPO, PS, and the PPO/PS blend were 212, 99.2, and 117°C, respectively. The composition of the blend was kept fixed for this study. The melt flow index was obtained with a 2.16-kg load at 190°C (usually used for thermoplastics) per ASTM D 1238.

The PPO/PS blend and organoclay were dried at 80°C in an air circulatory oven for 2 h before mixing to remove any residual desorbable moisture. The PPO/PS blend and Cloisite 10A (2, 4, or 6 wt % in each hybrid) were melt-mixed at 180°C in a Haake Rheocord (Waltham, MA) ($\sim$ 50-g scale) batch mixer at a mixing speed of 60 rpm for a time period of 10 min. Initially, for the first set of studies, processing was done at 220°C. However, the wide-angle X-ray diffraction (WAXD) data revealed degradation of the organic modifier at this processing temperature (as evidenced by a decrease in the *d*-spacing from the value for the organoclay after processing). Hence, a lower processing temperature of 180°C was used, which we found to be very suitable for the formation of nanocomposites with Cloisite 10A in a batch mixer and lower than the temperatures typically used for the processing of this blend. The processing temperature of 180°C is known not to promote degradation from previous studies in the literature for such types of organoclays, for thermoplastics such as PS and PMMA, and also for polypropylene. These processing conditions are suitable for mixing in terms of the pressure and melting temperature

developed during the processing period in the internal mixer.

Characterization of the nanocomposites

WAXD

The intercalation of the molecularly compatible (miscible) PPO/PS blend between the clay layers was confirmed by WAXD measurements. WAXD patterns were recorded on a Rigaku (Tokyo, Japan) diffractometer with Cu Kα radiation (wavelength = 1.5418 Å) at 40 kV and 100 mA. The experiments were performed in a scan range of 2θ = 2–14° with step increments of 0.05 at a speed of 2°/min on compression-molded samples. The scan range was sufficient to cover the intercalated region as well any region having clay stacks left unintercalated. The scan speed range of 0.5–5°/min for nanocomposites has been typically used previously in the literature.[16,17] The selected scan speed of 2°/min in our study was found to be sufficient to cover all data points. Too low a scan rate consumes unnecessary time, whereas too high a scanning rate increases noise in the curve without improving feature derivation in keeping with requirements posed by such intercalated samples.

Transmission electron microscopy (TEM)

TEM was performed on ~ 50–70-nm-thick sections obtained with a Leica Ultracut UCT microtome (Vienna, Austria). The sections were cut with a diamond knife at room temperature. Sections were collected on 300-mesh carbon-coated copper grids and dried overnight. TEM imaging was done with a JEOL (Tokyo, Japan) 1200EX electron microscope operating at an accelerating voltage of 80 kV. At least 10–15 images per sample were analyzed at each clay loading. Images were captured with a charged couple detector camera and viewed with Gatan digital micrograph software (Gatan Inc., Warrendale, PA).

Differential scanning calorimetry (DSC)

T_g was determined on a PerkinElmer (Waltham, MA) DSC-7 differential scanning calorimeter. The differential scanning calorimeter was calibrated with indium and sapphire as standards, and nitrogen flow through the DSC cell was maintained at 20 mL/min. The empty furnace was heated till 600°C and kept at this temperature for 10 min to remove any impurity if present. Scanning was done without a sample to obtain the baseline curve, which was then used for baseline correction. Samples of approximately 5–7 mg were measured in an aluminum pan of 40-μL capacity. Both the sample and reference pan were heated at 10°C/min from 50 to 170°C to relieve any thermal history of the glassy state. The heating rate of 10°C/min was used because it is a well-established heating rate to determine the T_g values of polymers and intercalated nanocomposites. The sample was allowed to cool to 50°C at a rate of 50°C/min and subsequently reheated from 50 to 170°C at the same rate of heating. The data obtained from the second scan were accepted to determine T_g.

Thermogravimetric analysis (TGA)

The onset of degradation at 10% weight loss (i.e., the temperature at 10% weight loss ($T_{10\%}$), the temperature at 50% weight loss ($T_{50\%}$), the maximum degradation temperature (T_{max}), and residue percentage for the PPO/PS blend and nanocomposites were determined with TGA. TGA was performed on a PerkinElmer TGA-7 instrument. Samples of about 4–4.5 mg were heated from 50 to 900°C at a heating rate of 10°C/min under a nitrogen atmosphere. The nitrogen flow rate was maintained at 20 mL/min. The selected temperature range was suitable to encompass the thermal degradation temperature of the polymer or its nanocomposites (sufficient to decompose volatiles present in the hybrids). The heating rate of 10°C/min was selected to maintain accuracy of data and to get smooth TGA curves without the loss of important features. A higher heating rate or sample weight would affect the degradation mechanism, resulting in the possibility of loss of accuracy in the results.[18] T_{max} values of the nanocomposites were determined from the differential thermogravimetry peak, which was obtained from the TGA curve with available Pyris (Waltham, MA) software.

RESULTS AND DISCUSSION

Intercalation structure by WAXD and TEM analysis

Initially, as a preliminary investigation to establish and confirm the suitability of the processing conditions for successful nanocomposite formation, the PPO/PS blend and Cloisite 10A organoclay were processed at 220°C (which is the usual and widely reported processing temperature for the PPO/PS blend) for a mixing time of 10 min at a speed of 60 rpm. For the nanocomposites prepared under these conditions, the WAXD results are presented in Table I. The negative change in the *d*-spacing from the organoclay to the PPO/PS–clay hybrid composite indicates a decrease in the clay gallery height due to the thermal degradation of organic modifier molecules. Also, a nanocomposite is not formed under these conditions as no polymer intercalation is observed. The decrease in the d_{001}-spacing was found to be in the range of 4–5 Å, which is significant for organically modified clays. The loss of the

TABLE I
d_{001}-Spacing (Å) Values for PPO/PS Blend Nanocomposite Samples with Various Clay Loadings Processed at 220°C

System	Clay loading[a]		
	2 wt %	4 wt %	6 wt %
PPO/PS–Cloisite 10A	14.4 (−4.6)	14.4 (−4.6)	15.0 (−4.0)

[a] The values in parentheses represent the difference between the d_{001}-spacings of the nanocomposite and clay (d_{001} for clay = 19.0 Å).

organic modifier from the organically modified clay at 220°C is responsible for the decrease in the d_{001}-spacing.[19] The resulting hybrids are conventional macrocomposites containing clay merely present as filler particles in the overall matrix. Therefore, to prevent thermal degradation and to facilitate successful nanocomposite formation by retention of the chemical species of the organic modifier, the processing temperature was lowered to 180°C while the mixing time and speed were kept at 10 min and 60 rpm, respectively. The results reported here and all further characterizations are for samples prepared at the processing temperature of 180°C. Table II lists the d_{001}-spacing values for successful and properly prepared PPO/PS blend nanocomposite samples. The processing temperature of 180°C results in successful intercalation of polymer chains between the layers of organically modified montmorillonite.

WAXD curves for PPO/PS nanocomposites are shown in Figure 1. The peak shifts toward lower 2θ values for all loadings, and this confirms the increase in the d_{001}-spacing of the organically modified montmorillonite by polymer intercalation. Although the d_{001}-spacing of the nanocomposite does not change much with the clay loading, as shown in Table II, the clay loading has a significant effect on the intensity of the peak as well as its width, as shown in Figure 1. The peak for PPO/PS nanocomposites with a 2 wt % clay loading has a relatively low intensity and is slightly broader. This may be due to the presence of some disordered clay layers in the PPO/PS blend matrix. As the level of the clay loading increases, the peak intensity increases because of the

TABLE II
d_{001}-Spacing and Calculated Number of Clay Platelets per Stack (N_c) for PPO/PS Blend Nanocomposite Samples with Various Clay Loadings Processed at 180°C

Clay (wt %)	d_{001} (Å)[a]	FWHM (rad)[b]	N_c
2	29.0 (10.0)	0.0136	4.1
4	31.0 (12.0)	0.0119	4.8
6	30.5 (11.5)	0.01	5.3

[a] The values in parentheses represent the difference between the d_{001}-spacings of the composite and clay.
[b] Full width at half-maximum.

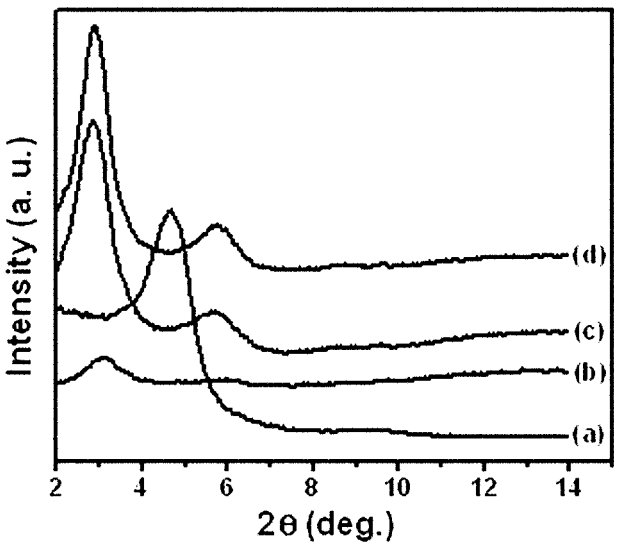

Figure 1 XRD curves of PPO/PS–Cloisite 10A nanocomposites with different clay loadings: (a) Cloisite 10A, (b) 2% Cloisite 10A, (c) 4% Cloisite 10A, and (d) 6% Cloisite 10A.

formation of intercalated nanocomposites without disruption of the multilayered order of clay layers, and this is not unexpected. More orientation order among clay layers is definitely likely at higher loadings, and this is seen as a peak with increased intensity. At a higher clay loading, a second-order peak also appears that may be due to a reduction in the interlamellar gallery height. However, high intensities show that a multiorder intercalated stack structure is well established in nanocomposites. The presence of a benzyl ring in the organic modifier improves the thermodynamic compatibility between organomontmorillonite and PS[20] and probably even PPO (as we expect from our results here), as PPO is molecularly compatible with PS.

The well-known Scherrer formula was employed to calculate the thickness (w) of the clay aggregates and to determine the mean number of platelets per stack for the nanocomposites at different clay loadings. The Scherrer formula is given as follows: $w = k\lambda/(B \cos \theta_B)$, where k is constant equal to 0.9, λ is the X-ray wavelength, $B \cong \theta_1 - \theta_2$ is the peak width at half-maximum intensity ($I_{max}/2$) in radians, and θ_B is the scattering angle. The number of clay platelets per stack can be calculated as $1 + w/d_{001}$. The results are tabulated in Table II. As shown in Table II, the number of clay platelets per stack is in the range of 4.1–5.3, which indicates that clay stacks with four to five platelets are dispersed in the PPO/PS matrix. This signifies that the morphology of the nanocomposites is well between intercalated and ideal exfoliation, along with a good level of dispersion. Although the number of clay platelets per stack is nearly the same at 4 and 6 wt % clay, the peak in-

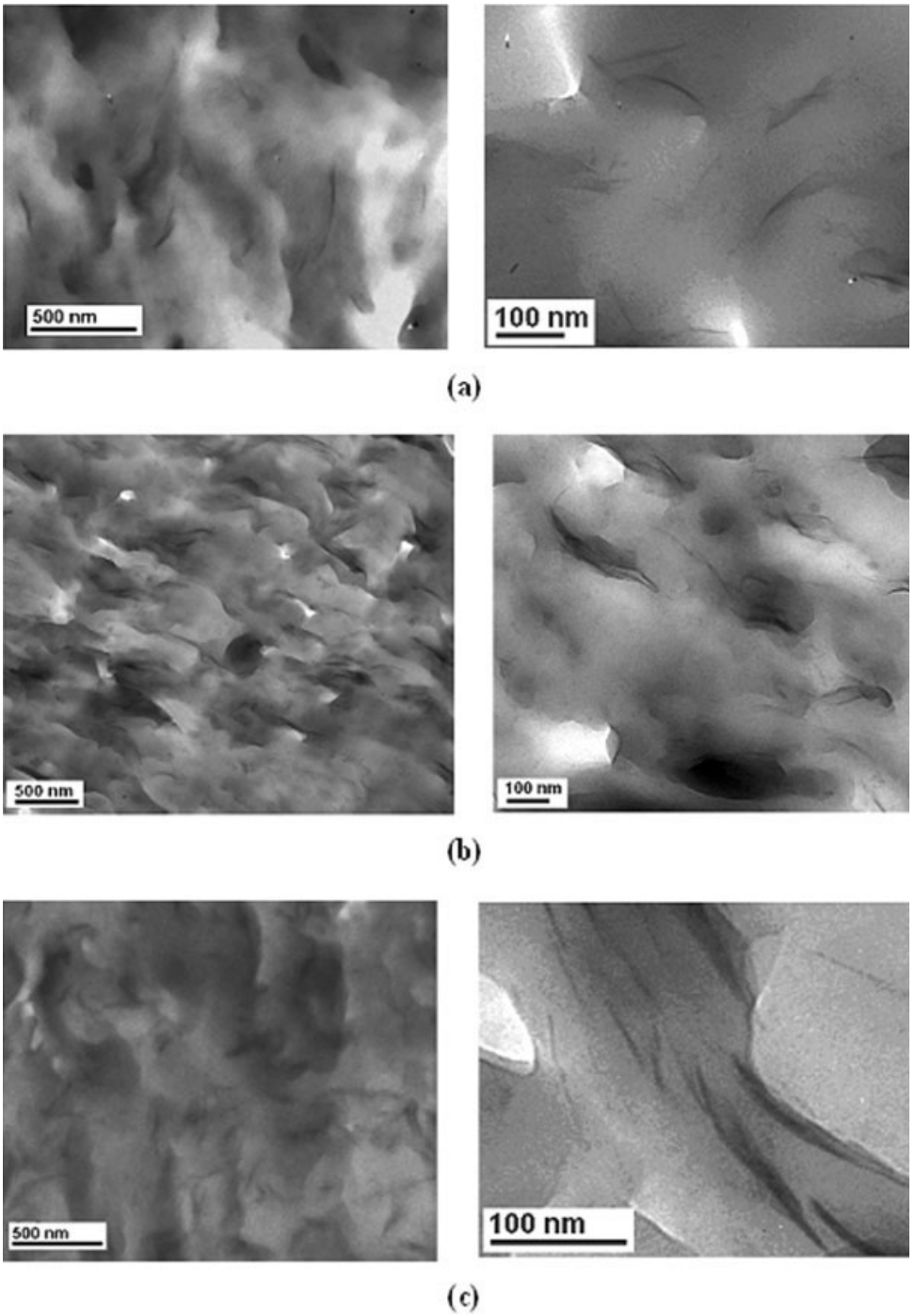

Figure 2 TEM micrographs of PPO/PS–Cloisite 10A nanocomposites: (a) 2% Cloisite 10A, (b) 4% Cloisite 10A, and (c) 6% Cloisite 10A.

tensity is higher at 6 wt % because of an increase in the number of clay stacks in the nanocomposites with the higher amount of clay.

Tanoue et al.[21] obtained intercalated nanocomposites of PS with Cloisite 10A using melt blending, and the d_{001}-spacing was shown to vary in the range of 4.0–4.9 nm, depending on the molecular weight of PS and the organoclay loading. The d_{001}-spacing for the high-molecular-weight PS nanocomposite with 2 wt % Cloisite 10A is 4.3 nm, which is $\sim$ 1.4 nm higher than our results here for the PPO/PS blend with the same clay loading. The higher change in the d_{001}-spacing in the case of PS nanocomposites may be due to high shear produced with the twin-screw extruder configuration used by the investigators in their work.[21] However, we still feel that the presence of a benzyl ring in Cloisite 10A forms favorable molecular thermodynamic interactions

TABLE III
T_g (°C) Values of PPO/PS Blend Nanocomposites with Different Organoclay Loadings

System	Clay loading			
	0 wt %	2 wt %	4 wt %	6 wt %
PPO/PS–Cloisite 10A	117	117.4	117.3	117.8

with both PPO and PS, leading to the intercalation of PPO and PS here. The thermodynamic interaction of PPO or PS with dimethyl benzyl hydrogenated tallow largely determines the extent of intercalation of PPO or PS within the clay galleries.

A previous report by Wang et al.[19] on the melt intercalation of PS into Cloisite 10A organoclay showed d_{001} values for the nanocomposite similar to those shown by this study. This suggests that the PPO/PS blend intercalates to the same extent as PS in Cloisite 10A with the same conditions and preparation method. This is rationalized to be due to the similar thermodynamic potential of PPO during intercalation along with PS with respect to this alkyl ammonium organoclay containing the favorable aliphatic segments (for delamination of clay) and benzyl groups (for interaction with PS as well as PPO). Our results also confirm those of Utracki et al.[21] for the PS–Cloisite 10A nanocomposite d_{001}-spacing. PPO has a shielding effect, preventing organic modifier degradation at 180°C, and the blend nanocomposites obtained by melt processing in a batch mixer are intercalated and homogeneously dispersed. The d_{001}-spacings from the study of Utracki et al. for PS–Cloisite 10A nanocomposites varied from 4.0 to 4.9 nm; however, we have obtained d_{001}-spacings of 2.9–3.1 nm for PPO/PS–Cloisite 10A nanocomposites. The extent of intercalation is not similar, possibly because of the use of high shear in their study. Vaia and Giannelis[22] showed by melt processing that PS intercalates into tetradecyl ammonium modified fluorohectorite (C14FH) and dioctadecyl dimethyl ammonium modified montmorillonite (2C18MT), resulting in only intercalated and partially exfoliated nanocomposites, respectively. The organoclays C14FH and 2C18MT, being fully aliphatic, should provide favorable interactions with the PPO/PS blend as well because of the molecular miscibility between PPO and PS, and it is therefore expected that the PPO/PS blend should also intercalate into C14FH and 2C18MT organoclays.

Figure 2(a–c) shows low- and high-magnification TEM images for PPO/PS–Cloisite 10A nanocomposites. At the low clay loading, the intercalated clay layers along with some individual clay layers leading to the formation of partially exfoliated nanocomposites can be observed. At a higher clay loading, the number of clay platelets per stack increases. Also, the number of clay stacks is greater at a higher clay loading, and this results in a higher intensity (WAXD curve peak) for the nanocomposites. Both WAXD and TEM measurements confirmed the formation of intercalated nanocomposites and the good dispersion of the clay layers and stacks within the blend matrix. We have not observed any appreciable difference in the clay particle distribution or the presence of large aggregates in different regions of the nanocomposite section. The TEM images in Figure 2 are representative of the whole nanocomposite bulk sample at each clay loading.

Thermal properties of the hybrids

The DSC data for PPO/PS blend nanocomposites at different clay loadings are shown in Table III. T_g of the blend clearly is not affected by the addition of clay until 6 wt %. Figure 3 shows overlapping DSC thermographs for the PPO/PS blend nanocomposite with Cloisite 10A. This reaffirms that our results for PPO/PS blend–clay hybrids are similar to the results obtained by Li and Ishida[23] for intercalated PS nanocomposites using hexadecyl ammonium modified montmorillonite by the solution method and melt-blending route; they observed the same T_g for nanocomposites as that of PS even at a 50% organoclay loading. We note that this similarity probably occurs on account of the high level of PS in the blend here because the dominant phase in the PPO/PS blend is PS. We also confirm that the bulk polymer outside the clay galleries principally contributes to T_g of the PPO/PS–clay nanocomposites. Vaia et al.[24] prepared melt-intercalated PS nanocomposites, using dioctadecyl dimethyl ammonium modified mica-type layered silicate, and they even observed an absence of T_g for the nanocomposite, which was attributed to the dimensional stability and resistance to flow by confined PS at a temperature above that of bulk PS.

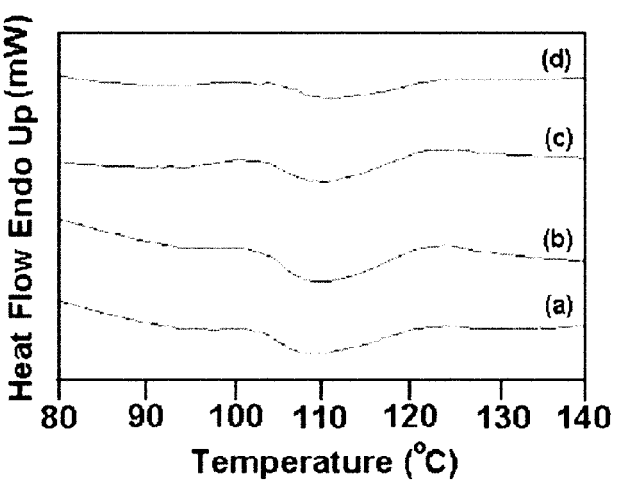

Figure 3 DSC overlay of PPO/PS–Cloisite 10A nanocomposites with different clay loadings: (a) Cloisite 10A, (b) 2% Cloisite 10A, (c) 4% Cloisite 10A, and (d) 6% Cloisite 10A.

TABLE IV
Comparison of the Thermal Stability of the PPO/PS Blend Nanocomposites and PPO/PS Blend

System	Clay loading (wt %)	Temperature (°C)			Residue (%)
		T_{10}	T_{50}	T_{max}	
PPO/PS	0	383	418	417	0
PPO/PS–Cloisite 10A	2	423	462	465	1.4
	4	413	451	449	2.9
	6	401	448	447	3.6

Such behavior has been observed for a melt-intercalated poly(ethylene oxide)–montmorillonite nanocomposite as well.[25] DSC and the more sensitive thermally simulated current technique have shown the absence of T_g for PS nanocomposites previously in the early literature on nanocomposites. However, the use of the thermally simulated current thermal sampling technique has shown a broad transition corresponding to a low degree of cooperative motion of polymer segments.[26] A decrease in T_g has also been observed in melt-processed PMMA–montmorillonite nanocomposites.[27]

The weight losses of organic matter in the blend and nanocomposites were determined with TGA. Table IV shows loss temperatures for 10 and 50 wt % losses of organic matter. T_{max} gives the value at the maximum rate of weight loss (% loss/min), which provides information on the maximum thermal stability of the nanocomposite. The residue (%) values are also reported. Figure 4 shows TGA curves for the blend and nanocomposites. The thermal stability of the nanocomposites is better than that of the blend. The onset of degradation for the nanocomposites is about 40°C higher at a low clay loading. However, no clear trend can be observed for the increase in the onset of degradation for the nanocomposites at different clay loadings. The overall thermal stability of the nanocomposite is higher by 30°C than that of the blend. The maximum improvement in the thermal stability has been observed at a 2 wt % clay loading. Cloisite 10A contains 35% excess organic modifier (cation-exchange concentration = 1.25 mequiv/g clay). The amount of the organic modifier increases with the clay loading, and this reduces the thermal stability of the nanocomposites at higher clay loadings. Zhu et al.[26] showed a significant improvement in the onset of degradation of PS nanocomposites with as little as 0.1 wt % clay. However, at a higher clay loading (>3 wt % clay), $T_{10\%}$ was found to level off. Zheng and Wilkie[28] showed an increase in the onset of degradation by 27–35°C, whereas the overall thermal stability was higher by 29–31°C for melt-processed nanocomposites of PS, polycaprolactone, and modified organoclay. Previous results in the literature are comparable to results from our study, and this is reaffirming and also understandable because of the presence of PS as the dominant phase in the blend here. Recently, Zhang et al.[29] reported an increase in the thermal stability for melt-processed intercalated nanocomposites of PS and oligomerically modified clay; the temperatures at 10 and 50 wt % degradation increased by 8 and 15°C, respectively, with 3 wt % clay.

Mechanical properties of the blend nanocomposites

Figure 5 shows the variation of Young's modulus of the nanocomposites with the clay loading. Young's modulus for the nanocomposites increases linearly until 4 wt % Cloisite 10A and levels off at higher clay loadings. The nanocomposite samples were brittle above 6 wt %. The organically modified montmorillonite improves the stiffness of the PPO/PS blend. Such a linear increase in the modulus with the clay loading has been observed for nanocomposites of various thermoplastic polymers such as PS[30] and polycarbonate.[31] Tanoue et al.[30] observed an increase in the modulus with the clay loading for a melt-processed PS–Cloisite 10A nanocomposite, whereas the break stress was observed to increase at 2 wt % and further decrease with the loading at higher clay fractions. Our

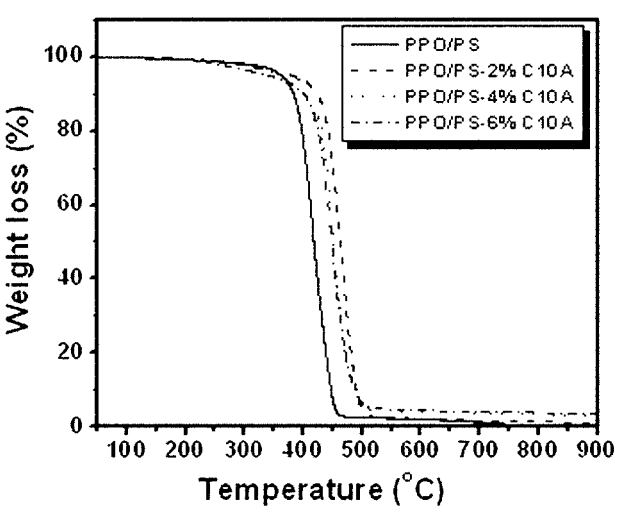

Figure 4 TGA thermographs of PPO/PS blend–Cloisite 10A nanocomposites with different clay loadings.

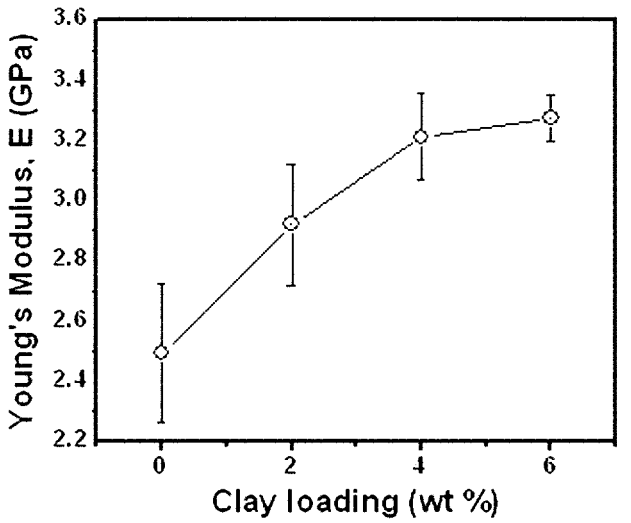

Figure 5 Variation of Young's modulus (GPa) for PPO/PS blend nanocomposites with different clay loadings.

results for the stress at break (tensile strength) show a decrease with an increase in the loading.

Figure 6 shows the variation of the break stress and break strain (%) with the clay loading. The break stress and break strain were found to decrease with an increase in the clay fraction, except at the 4 wt % clay loading, at which a slight increase in both properties can be seen. Interestingly, both the break stress and break strain show similar qualitative behavior with the clay loading. The decrease in the break stress and break strain results from the brittleness (reduction in ductility) caused by the inclusion of clay in the polymer blend matrix.

Modulus comparison with the Halpin–Tsai model prediction

The Scherrer equation (with WAXD curves) was used to calculate the globally averaged mean stack thickness and the number of clay platelets per stack for the nanocomposites. The average stack length was measured from TEM images with 150–180 counts. The counts were taken from different regions on the grid. High- and low-magnification images were used for particle length calculation. The stack length for the nanocomposites is 127 nm. It has been found that the stack length variation is small in the range of clay loadings studied here. The filler aspect ratio changes from 14.1 at a 2 wt % clay loading to 9.5 at a 6 wt % clay loading. It is unlikely that the aspect ratio will influence the Halpin–Tsai calculation, and this is also shown in Figure 7 and discussed as follows.

The peak intensity for a nanocomposite increases with the clay fraction, whereas increases in the full width at half-maximum and number of platelets per stack are not significant as a function of the clay fraction; this suggests clearly that the level of dispersion of the clay stack within the polymer matrix is unaffected by the clay loading. As the aspect ratio and dispersion of clay stacks are not varying in the nanocomposites at various levels of the filler concentration, the increase in the modulus is principally due to the reinforcing effect of the filler and amount of intercalated polymer.

The Halpin–Tsai theory and model, which are generally used for predicting the stiffness of unidirectional composites as a function of the aspect ratio,[32–34] have been used in our study to show that this model in particular fits the experimental data on the modulus very well. As described here, this model, using minimum parameters obtained from experimentally derived filler dispersion data, can be

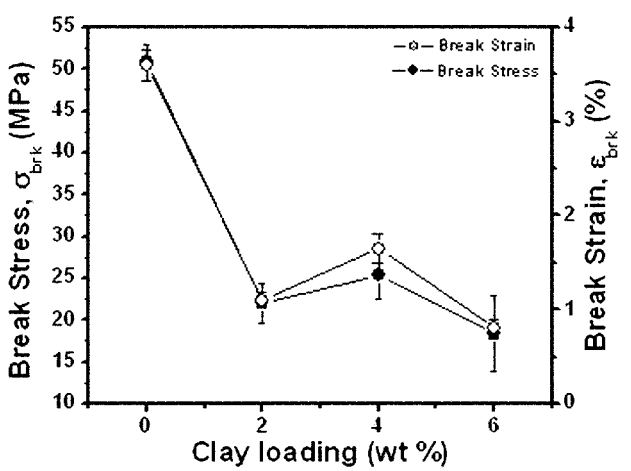

Figure 6 Variation of the break stress (MPa) and break strain (%) for PPO/PS blend nanocomposites with different clay loadings.

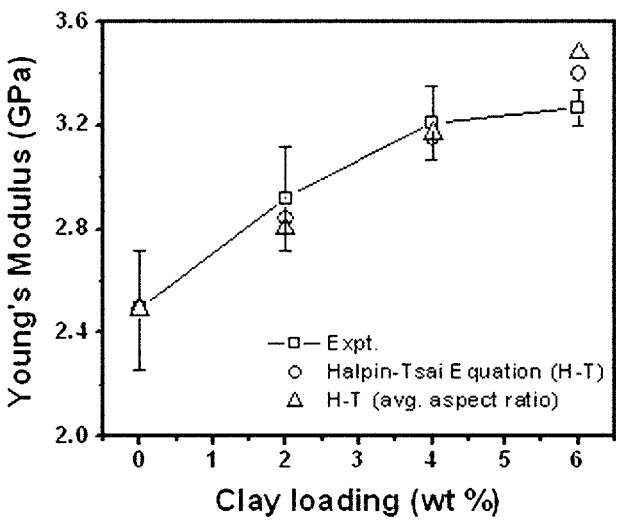

Figure 7 Comparison of Young's modulus (GPa) for PPO/PS blend nanocomposites from experimental measurements and Halpin–Tsai model fits. Halpin–Tsai fits are shown by the use of an individual aspect ratio and average aspect ratio over all clay loadings.

TABLE V
Comparison of the Experimental and Theoretically Modeled Mechanical Moduli with Various Clay Loadings

Clay (wt %)	d_{001} (Å)[a]	N_c[b]	Stack thickness (Å)	Aspect ratio	E_{stack} (GPa)[c]	E_{expt} (GPa)[d]	E_{H-T} (GPa)[e]	E_{H-T} (GPa)[f]	E_{H-T} (GPa)[g]
2	29.0 (10.2)	4.1	89.9	14.1	70.6	2.92 ± 0.2 (17.3%)	2.84	2.80	3.98
4	31.0 (12.0)	4.8	117.0	10.8	64.7	3.21 ± 0.14 (28.9%)	3.15	3.17	5.51
6	30.5 (11.5)	5.3	134.0	9.5	64.9	3.27 ± 0.07 (31.3%)	3.40	3.48	7.06

The theoretical parameters are from the Halpin–Tsai model.
[a] The values in parentheses represent the difference between the d_{001}-spacings of the composite and clay.
[b] Number of clay platelets per stack.
[c] Young's modulus of the clay stack.
[d] Young's modulus determined experimentally (values in parentheses show the percentage increase in the modulus with respect to the unfilled blend).
[e] Young's modulus determined with the Halpin–Tsai model.
[f] Young's modulus determined with the Halpin–Tsai model (average aspect ratio).
[g] Young's modulus determined with the Halpin–Tsai model (complete exfoliation).

used to quantitatively predict the modulus of the blend nanocomposites satisfactorily. Young's modulus is expressed as follows:

$$\frac{E}{E_m} = \frac{1 + \xi\eta\phi}{1 - \eta\phi} \tag{1}$$

where E and E_m represent Young's moduli of the composite and matrix, respectively; ξ = (2 × aspect ratio) is a shape parameter, and ϕ is the filler volume fraction. η is determined as follows:

$$\eta = \frac{(E_f/E_m) - 1}{(E_f/E_m) + \xi} \tag{2}$$

where E_f represents Young's modulus of the filler. The aspect ratio values were obtained from the WAXD curves (platelet thickness with the Scherrer equation), and the stack length (averaged) was obtained from TEM images.

The tensile modulus of the stack (E_{stack}) in the direction parallel to its platelets can be calculated as follows:

$$E_{stack} = \phi_{MMT}E_{MMT} + \phi_{gallery}E_{gallery} \tag{3}$$

where ϕ_{MMT} is the volume fraction of silicate (montmorillonite) layers in the clay stack, E_{MMT} is the modulus of montmorillonite, $\phi_{gallery}$ is the volume of the gallery space (interlayer), and $E_{gallery}$ is the modulus of the material in the gallery.[35,36] $\phi_{gallery}$ is the ratio of the total gallery thickness to the total stack thickness:

$$\phi_{gallery} = \frac{(N_c - 1)(d_{001} - t_{platelet})}{d_{001}(N_c - 1) + t_{platelet}} \tag{4}$$

where N_c is the number of platelets per stack, d_{001} is the d-spacing for the nanocomposite, and $t_{platelet}$ is the thickness of the silicate platelet.

The modulus for the montmorillonite platelet was taken to be 178 GPa.[36,37] The modulus for PPO/PS was found to be 2.49 GPa from our present measurements. The stack modulus does not vary significantly with the clay loading as the number of clay platelets per stack and d_{001} spacing for the nanocomposites do not change significantly with the clay loading. With these parameters, the moduli for the nanocomposites were calculated, and they are tabulated in Table V. The modulus of the material in the interlayer gallery (organic modifier and polymer) can be neglected as it is very low compared to the modulus of the clay platelet. However, the number of platelets per stack, the d-spacing, and the volume fraction of the interlayer spacing per clay stack change with the clay loading, and these therefore affect the modulus of a clay stack, thus leading to the stack modulus changing with the change in the clay fraction in the nanocomposite.

The Halpin–Tsai theory predicts a modulus value of the nanocomposites comparable to that obtained from experimental results, except for the higher level 6 wt % clay loading, at which there is some deviation. Although the aspect ratio is slightly lower at 6 wt %, the equation predicts a slightly higher modulus. Furthermore, when the experimentally obtained aspect ratio values were averaged over all clay loadings (2, 4, and 6 wt %) and used as a constant parameter in the Halpin–Tsai equation, the predicted modulus value was found to slightly decrease at 2 wt % clay and increase slightly at 6 wt %. These changes, however, are not significant. At any particular loading value, qualitatively an increase in the aspect ratio increases Young's modulus. With the Halpin–Tsai model, the modulus of the nanocomposite was also calculated, assuming an idealized completely exfoliated system for the purpose of comparison. These values are given in Table V. The modulus values for the completely exfoliated system are 36–115% higher over the 2–6 wt % range. The values of

Young's modulus calculated from the theory and experiments are shown in Figure 7 as a function of the clay loading, and good agreement between the experimental data and theoretical calculations can be observed.

CONCLUSIONS

New intercalated and dispersed PPO/PS blend nanocomposites with organically modified clay were prepared with a melt-mixing method under appropriate processing conditions, which included a lower melt temperature compared to the conventional condition for this fundamentally interesting and industrially important miscible polymer blend. The effects of the clay loading on the nanoscale and mesoscale structures, morphology, and thermal and mechanical properties are investigated to the best of our knowledge for the first time here. WAXD shows a significant amount of penetration of PPO and PS chains between the silicate layers. The lower processing temperature (180°C) prevents degradation of the organic modifier, which is necessary for polymer intercalation between the clay layers. The change in the d_{001}-spacing due to polymer intercalation is 12 Å over the 2–6 wt % range of clay fractions studied. The level of intercalation for PPO/PS blend nanocomposites in our present study is quite comparable to that reported in the literature for PS nanocomposites prepared with the same organoclay. This is mainly due to the same molecular thermodynamic potential of PPO along with intercalating PS, both of which form favorable interactions with the aliphatic and benzyl groups and segments of the organoclay.

These nanocomposites show negligible change in T_g, as measured by DSC, and this is similar to results previously reported for melt-processed PS nanocomposites in the literature. The thermal stability of the nanoscale hybrids is higher than that of the blend, as determined by TGA. The onset of degradation for these blend–clay nanocomposites increases by 40°C, whereas the overall thermal stability is improved by 48°C; this is similar to the observations made for PS nanocomposites prepared by melt processing and reported previously in the literature. Hence, we also conclude that in this particular case of new miscible blend–clay intercalated nanocomposites, the compositionally dominant polymer phase in the blend controls the thermal degradation behavior. The mechanical tensile modulus of the nanocomposites varies roughly linearly with the clay fraction, as has been observed for hybrids with other thermoplastic polymers previously, and the value of the modulus increases by 31% with 6 wt % organoclay. The experimentally measured modulus compares very well with theoretical values calculated with the Halpin–Tsai model with aspect ratios used from the experimental measurements (WAXD and TEM). With the aspect ratio of the clay stacks remaining roughly constant over the range of filler loadings, a single value could also be used successfully to predict the modulus as a function of loading without the need for experimentally derived parameters at each level of clay fraction in the matrix. The tensile strength (break stress) and the maximum elongation (break strain) decrease with an increase in the clay loading, and this is not unusual for intercalated thermoplastic–clay nanocomposites.

The authors are thankful to Southern Clay Products, Inc. (Texas, USA), and appreciate the generous gift of the clay samples. The assistance provided by R. S. Gholap with the transmission electron microscopy imaging is very much appreciated.

References

1. Giannelis, E. P. Adv Mater 1996, 8, 29.
2. Giannelis, E. P.; Krishnamoorti, R.; Manias, E. Adv Polym Sci 1999, 138, 107.
3. LeBaron, P. C.; Wang, Z.; Pinnavaia, T. J Appl Clay Sci 1999, 15, 11.
4. Alexandre, M.; Dubois, P. Mater Sci Eng 2000, 28, 1.
5. Yano, K.; Usuki, A.; Karauchi, T.; Kamigaito, O. J Polym Sci Part A Polym Chem 1993, 31, 2493.
6. Usuki, A.; Kojima, Y.; Kawasumi, M.; Okada, A.; Fukushima, Y.; Kurauchi, T.; Kamigaito, O. J Mater Res 1993, 8, 1174.
7. Li, Y.; Shimizu, H. Polymer 2004, 45, 7381.
8. Gelfer, M. Y.; Song, H. H.; Liu, L.; Hsiao, B. S.; Chu, B.; Rafailovich, M.; Si, M.; Zaitsev, V. J Polym Sci Part B: Polym Phys 2003, 41, 44.
9. Brandrup, J.; Immergut, E. H. Polymer Handbook, 3rd ed.; Wiley-Interscience: New York, 1989.
10. Hammel, R.; Macknight, W. J.; Karasz, F. E. J Appl Phys 1975, 46, 4199.
11. Runt, J. P. Macromolecules 1981, 14, 420.
12. Chun, B. C.; Gibala, R. Polym Eng Sci 1996, 36, 744.
13. Tjong, S. C.; Ke, Y. C. Polym Eng Sci 1996, 36, 2626.
14. Malik, T. M.; Carreau, P. J.; Chapleau, N. Polym Eng Sci 1989, 29, 600.
15. Costa, D. A.; Oliveira, C. M. F. Polym Test 1994, 13, 205.
16. Yasmin, A.; Abot, J. L.; Daniel, I. M. Mater Res Soc Symp Proc 2003, 740, 13.7.10.
17. Ratanarat, K.; Nithitanakul, M.; Martin, D. C.; Magaraphan, R. Rev Adv Mater Sci 2003, 5, 187.
18. Carrasco, F.; Pagès, P. J Appl Polym Sci 1996, 61, 187.
19. Wang, D.; Zhu, J.; Yao, Q.; Wilkie, C. A. Chem Mater 2002, 14, 3837.
20. Doh, J. G.; Cho, I. Polym Bull 1998, 41, 511.
21. Tanoue, S.; Utracki, L. A.; Rejon, A. G.; Tatibouët, J.; Cole, K. C.; Kamal, M. R. Polym Eng Sci 2004, 44, 1046.
22. Vaia, R. A.; Giannelis, E. P. Macromolecules 1997, 30, 8000.
23. Li, Y.; Ishida, H. Macromolecules 2005, 38, 6513.
24. Vaia, R. A.; Ishii, H.; Giannelis, E. P. Chem Mater 1993, 5, 1694.
25. Vaia, R. A.; Sauer, B. B.; Tse, O. K.; Giannelis, E. P. J Polym Sci Part B: Polym Phys 1997, 35, 59.
26. Zhu, J.; Morgan, A. B.; Lamelas, F. J.; Wilkie, C. A. Chem Mater 2001, 13, 3774.

27. Kumar, S.; Jog, J. P.; Natarajan, U. J Appl Polym Sci 2003, 89, 1186.
28. Zheng, X.; Wilkie, C. A. Polym Degrad Stab 2003, 82, 441.
29. Zhang, J.; Jiang, D. D.; Wang, D.; Wilkie, C. A. Polym Adv Technol 2005, 16, 800.
30. Tanoue, S.; Utracki, L. A.; Rejon, A. R.; Tatibouët, J.; Kamal, M. R. Polym Eng Sci 2005, 45, 827.
31. Yoon, P. J.; Hunter, D. L.; Paul, D. R. Polymer 2003, 44, 5323.
32. Halpin, J. C. J Compos Mater 1969, 3, 732.
33. Halpin, J. C.; Kardos, J. L. Polym Eng Sci 1976, 16, 344.
34. Ashton, J. E.; Halpin, J. C.; Petit, P. H. Primer on Polymer Composite Materials: Analysis; Technomic: Stanford, CT, 1969.
35. Brune, D. A.; Bicerano, J. Polymer 2002, 43, 369.
36. Fornes, T. D.; Paul, D. R. Polymer 2003, 44, 4993.
37. Alexandrov, K. S.; Ryshova, T. V. Bull Acad Sci USSR Geophys Ser 1961, 12, 1165.